Signal-to-Interference-Plus-Noise Ratio Analysis for Direct-Sequence Ultra-Wideband Systems in Generalized Saleh–Valenzuela Channels

Wei-De Wu, *Student Member, IEEE*, Cheng-Chia Lee, Chung-Hsuan Wang, *Member, IEEE*, and Chi-chao Chao, *Member, IEEE*

***Abstract*—In this paper, exact signal-to-interference-plus-noise ratio (SINR) analysis of direct-sequence ultra-wideband (UWB) systems with Rake receiving in the presence of inter-symbol interference and multiple-access interference over a generalized Saleh–Valenzuela (GSV) channel with a generic pulse shaping function is provided. The SINR expression, for synchronized multiple-access, is first obtained without assuming random spreading. The GSV channel structure under consideration is a generalization of the Saleh–Valenzuela channel structure with generalized path-gain and path-arrival models, examples of which can include all the IEEE 802.15.3a UWB channel models and some of the IEEE 802.15.4a models. Then, by the novel treatment of renewal processes, the exact average SINR over the GSV channel statistics is obtained. Our analytical results well match computer simulations and can readily be applied to evaluate and improve the performance of UWB systems over realistic channel and interference models.**

***Index Terms*—Direct-sequence (DS), generalized Saleh–Valenzuela (GSV) channel, Poisson process, renewal process, signal-to-interference-plus-noise ratio (SINR), ultra-wideband (UWB).**

I. Introduction

INCREASING demands for higher-rate wireless communications have induced the need for more advanced communication technologies. One very promising candidate is called ultra-wideband (UWB), which is characterized as a signaling technique with ultra-wide signal bandwidth and reduced power spectral density [1]. Owing to its ultra-wide bandwidth, a UWB system has potential advantages over conventional systems, such as robustness to multipath fading, coexistence with other systems using the same band, high data rate capability, and fine time resolution [2]–[5].

Manuscript received November 30, 2006; revised July 12, 2007. This work was supported by the National Science Council of the Republic of China under Grants NSC 94-2213-E-007-027 and NSC 95-2219-E-007-003. This paper was presented in part at the IEEE Wireless Communications and Networking Conference, Hong Kong, March 2007. The associate editor coordinating the review of this manuscript and approving it for publication was Prof. Alle-Jan van der Veen.

W.-D. Wu and C. Chao are with the Institute of Communications Engineering, National Tsing Hua University, Hsinchu 30013, Taiwan, R.O.C. (e-mail: weide.wu@gmail.com, ccc@ee.nthu.edu.tw).

C.-C. Lee is with the Sunplus mMobile Inc., Hsinchu 30076, Taiwan, R.O.C. (e-mail: chengchia.lee@sunplusmm.com).

C.-H. Wang is with the Department of Communication Engineering, National Chiao Tung University, Hsinchu 30010, Taiwan, R.O.C. (e-mail: chwang@mail.nctu.edu.tw).

Color versions of one or more of the figures in this paper are available online at http://ieeexplore.ieee.org.

Digital Object Identifier 10.1109/JSTSP.2007.906642

Despite the progress in UWB technology, there is still considerable uncertainty over the parameters of what will constitute successful UWB designs and deployment. This can be caused by the difficulty to take into account the unique path-arrival statistics in UWB channels [6], such as those modified from the Saleh–Valenzuela (SV) channel model [7] and adopted by IEEE 802.15.3a [8], [9] and 802.15.4a Task Groups [10], [11]. In [8], a channel is described by two Poisson processes of cluster and ray arrivals. The inter-arrival time of the ray arrival process is further generalized to possess a mixed exponential distribution in [10]. It is clear that successful UWB designs and deployment should be able to exploit the channel statistics, but we notice that few analytical results with realistic UWB channel models have been provided in the literature.

Nevertheless, concerning the performance analysis of spread-spectrum (SS) UWB systems [12], [13], the average output signal-to-interference-plus-noise ratio (SINR) of a time-hopping SS UWB system with Rake receiving over IEEE 802.15.3a channel models has been provided in [14]. The cluster and ray arrival processes, modeled as Poisson processes, are approximated by binomial random sequences under the assumption of very fine channel resolution. The approximation can, however, become inaccurate with coarser channel resolution, and the inter-symbol interference (ISI) is ignored in [14]. A more precise analysis for SS UWB systems with maximal-ratio-combining over IEEE 802.15.3a channel models has been conducted in [15] while the effect of the pulse function is simplified as a rectangular window and neither ISI nor multiple-access interference (MAI) is considered. In [16], a computable bit-error rate formula is provided by deriving the moment-generating function of the sum of combined path gains in a given observation window. The result is further extended in [17] to take the shadowing effect and configurations of a Rake receiver into consideration and in [18] for IEEE 802.15.4a channel models. However, no interference has been taken into account in [16]–[18]. Although [19] and [20] have provided some useful analytical results to characterize the statistics of IEEE 802.15.3a channel models, they are still not adequate for performance analysis regarding interferences, such as ISI, and generic pulse shaping functions. For impulse radio UWB systems employing correlation receivers, e.g., transmitted reference systems [21], performance evaluation regarding inter-frame and multiuser interferences has been carried out by utilizing some channel-related decay profile functions [22]–[24], where, however, the profile functions are only obtained over measurement data or a simplified channel

1932-4553/$25.00 © 2007 IEEE

model. Consequently, consideration of both the interferences and realistic UWB channel models have not been completely addressed in the previous works [14]–[20], [22]–[24].

In this paper, we propose an analytical framework based on the novel treatment of *renewal processes* [25], [26] to derive an exact analytical expression of the average output SINR for a direct-sequence (DS) UWB system with Rake receiving. The investigated system model includes the realistic presence of both ISI and MAI. The SINR expression, under consideration of the code correlation functions, a Rake receiver with variable number of combining fingers, and arbitrary channel correlations, is first derived without assuming random spreading, which was usually assumed in the literature, e.g., [27], [28]. The discrete-time baseband channel considered is generated and converted from a generalized Saleh–Valenzuela (GSV) channel regarding the effect of a generic pulse shaping function, where the GSV channel structure is an extension of the SV model [7] with generalized path-gain and path-arrival models. Then, by treating the cluster and ray arrivals as renewal processes, the exact average SINR over channel statistics is obtained. Our analytical results well match computer simulations and can readily be used to evaluate and improve the performance of DS-UWB systems over realistic channel and interference models. It is noticed that, by virtue of the generic channel structure investigated, our analysis can cover many UWB channel models of interest, including all the IEEE 802.15.3a channel models and some of the IEEE 802.15.4a models with clustering phenomena.[1]

This paper is organized as follows. In Section II, system and channel models are introduced. The SINR expression, before averaged over the channel statistics, is derived in Section III. In Section IV, the exact average SINR is obtained by exploiting the properties of renewal processes. Analytical and simulation results are then given and compared in Section V. Finally, concluding remarks are drawn in Section VI.

II. System and Channel Models

In this section, the considered DS-UWB system and channel models are introduced. To reflect practical system operations, we consider the equivalent discrete-time baseband models.

A. DS-UWB System

The transmitted signal of the νth user in a DS-UWB system assumes the following format:

$$s^{(\nu)}[n] = d^{(\nu)}_{\lfloor n/N_c \rfloor} c^{(\nu)}[n]$$

where $\left\{d_k^{(\nu)}\right\}_{k\in\mathbb{Z}}$ denote the modulated data symbols with mean zero and $E\left\{d_k^{(\nu)} d_{k'}^{(\nu')*}\right\} = E_s$ only when $k = k'$ and $\nu = \nu'$ and zero, otherwise. $c^{(\nu)}[n]$ represents an infinite periodic spreading sequence with period N_c and $\sum_{n=0}^{N_c-1} |c^{(\nu)}[n]|^2 = 1$. Assuming N_u synchronized co-channel users,[2] we can express the discrete-time baseband received signal as

$$r[n] = \sum_{\nu=1}^{N_u} \sum_{l=0}^{L-1} h^{(\nu)}[l] s^{(\nu)}[n-l] + \eta[n]$$

where $\{h^{(\nu)}[n]\}_{n=0}^{L-1}$ denote the tap coefficients of a length-L channel experienced by $s^{(\nu)}[n]$ and $\eta[n]$ is the complex Gaussian random sequence with mean zero and $E\{\eta[n]\eta^*[n']\} = N_0\delta[n-n']$, representing the effect of the additive white Gaussian noise. Note that $\delta[n] = 1$ when $n = 0$ and zero, otherwise.

Without loss of generality, assume that user 1 is the desired user and $d_0^{(1)}$ is to be detected by forming the following decision variable:

$$Z = \sum_{i=0}^{L-1} \tilde{h}^*[i] \sum_{n=0}^{N_c-1} c^*[n] r[n+i] \tag{1}$$

where

$$\tilde{h}[i] = \begin{cases} h[i], & 0 \le i \le N_f - 1 \\ 0, & \text{otherwise} \end{cases}$$

and all the superscripts corresponding to the desired user 1 will be dropped hereinafter for notation simplicity. Note that (1) corresponds to the combining operation in a Rake receiver with N_f fingers. In Section III, we will further investigate the interference parts in (1).

B. Discrete-Time Baseband Channel From GSV Channel Structure

The considered discrete-time baseband channel is obtained from the GSV channel structure, where a random channel realization consists of clusters of random arriving rays

$$h(t) = \sum_{l\ge 0} \sum_{k\ge 0} \alpha(T_l, \tau_{k,l}) \delta(t - T_l - \tau_{k,l}) \tag{2}$$

where $\delta(t)$ is the Dirac delta function, T_l is the arrival time of the first ray in the lth cluster, and $\tau_{k,l}$ denotes the delay time of the kth ray in the lth cluster relative to T_l. And $\alpha(T_l, \tau_{k,l})$ is the path gain of the kth ray in the lth cluster, satisfying that

$$E\left\{\alpha(T_l,\tau_{k,l})\alpha^*(T_{l'},\tau_{k',l'}) \middle| T_l, \tau_{k,l}, T_{l'}, \tau_{k',l'}\right\} = \begin{cases} \Omega_0 e^{-T_l/\Gamma} e^{-\tau_{k,l}/\gamma}, & \text{if } T_l = T_{l'} \text{ and } \tau_{k,l} = \tau_{k',l'} \\ 0, & \text{otherwise} \end{cases} \tag{3}$$

and the fourth-order joint moment,

$$E\left\{\alpha(T_{l_1},\tau_{k_1,l_1})\alpha^*(T_{l_2},\tau_{k_2,l_2})\alpha(T_{l_3},\tau_{k_3,l_3})\alpha^*(T_{l_4},\tau_{k_4,l_4}) \middle| T_{l_j}, \tau_{k_j,l_j}, j = 1,\ldots,4\right\}$$

can be nonzero only if $(l_1,k_1) = (l_2,k_2) = (l_3,k_3) = (l_4,k_4)$ or $(l_1',k_1') = (l_2',k_2')$ and $(l_3',k_3') = (l_4',k_4')$ where (l_j',k_j'), $j = 1,\ldots,4$, is a relabeling

[1] This paper is extended from a previous conference version [29], where only preliminary results for IEEE 802.15.3a channel models with idealized effect of pulse shaping functions are provided.

[2] The synchronized assumption can be realized by applying some synchronizing methods, e.g., those in [30], [31] with novel signaling and receiving designs. Nevertheless, it is possible to extend the following analysis to asynchronized cases, as will be commented in Section VI.

of (l_j, k_j), $j = 1, \ldots, 4$. Also Ω_0 is the mean energy of the first ray in the first cluster, and Γ and γ denote the cluster and ray decay factors, respectively. For ease of the following analysis, we also require the following ratios to be constant:

$$r_2 = \frac{E\left\{|\alpha(T_l, \tau_{k,l})|^2 |\alpha(T_l, \tau_{k',l})|^2 \middle| T_l, \tau_{k,l}, \tau_{k',l}\right\}}{E\left\{|\alpha(T_l, \tau_{k,l})|^2 \middle| T_l, \tau_{k,l}\right\} E\left\{|\alpha(T_l, \tau_{k',l})|^2 \middle| T_l, \tau_{k',l}\right\}} \tag{4}$$

$$r_4 = \frac{E\left\{|\alpha(T_l, \tau_{k,l})|^4 \middle| T_l, \tau_{k,l}\right\}}{\left(E\left\{|\alpha(T_l, \tau_{k,l})|^2 \middle| T_l, \tau_{k,l}\right\}\right)^2} \tag{5}$$

for all k, k', l.[3] Note that, the path loss, frequency-dependent decay, shadowing effects, etc., are not included in the path-gain model since we mainly focus on the multipath effect.

According to the realistic channel measurements [7], [8], [10], the cluster inter-arrival times, $\{T_l - T_{l-1}\}_{l \geq 1}$, are assumed to be independent and identically distributed (i.i.d.) exponential random variables (RVs) of parameter Λ with probability density function (pdf):

$$f_c(x) = \Lambda e^{-\Lambda x}. \tag{6}$$

The initial cluster arrival time, T_0, follows the same distribution whenever there is no line-of-sight (LOS) but it is set to zero if LOS is present. The ray inter-arrival times, $\{\tau_{k,l} - \tau_{k-1,l}\}_{k \geq 1}$, are, on the other hand, assumed to be i.i.d. RVs with a more generic pdf

$$f_r(x) = \beta \cdot \lambda_1 e^{-\lambda_1 x} + (1 - \beta) \cdot \lambda_2 e^{-\lambda_2 x} \tag{7}$$

where $0 < \beta \leq 1$. The initial ray arrival times $\tau_{0,l} = 0$, for all l, i.e., there is always a ray when a cluster begins. Note that, when $\beta = 1$, (7) is reduced to an exponential pdf of parameter λ_1.

The GSV channel structure described by (2)–(7) can comprise many channel models of interest. For example, when $\{\alpha(T_l, \tau_{k,l})\}$ are complex Gaussian RVs, the cluster and ray inter-arrival times assume exponential distributions of parameters Λ and λ_1, respectively, and, if $T_0 = 0$, one can obtain the complex baseband channel structure defined in [7]. When $\{\alpha(T_l, \tau_{k,l})\}$ are further modified to be real-valued RVs with log-normal distributed magnitude and equally probable positive and negative signs and T_0 is chosen according to the presence of LOS, we have the IEEE 802.15.3a passband channel structure, in absence of the shadowing effect, described in [8], [9]. The values of r_2 and r_4 can be found to be, respectively, $e^{(\ln 10/10)^2 \sigma_1^2}$ and $e^{(\ln 10/10)^2 \left(\sigma_1^2 + \sigma_2^2\right)}$, where σ_1 and σ_2 are constants defined in [8]. For IEEE 802.15.4a channel models specified in [10], [11], excluding CM4 and CM8 of the tap-delay-line structure and CM7 of ray decay factor γ varying with the cluster arrival times, $\{\alpha(T_l, \tau_{k,l})\}$ are RVs with magnitude of Nakagami-m distribution[4] and uniform random phase, and one can have $r_2 = e^{(\ln 10/10)^2 \sigma_{\text{cluster}}^2}$ and $r_4 = e^{(\ln 10/10)^2 \sigma_{\text{cluster}}^2} \left(1 + e^{-m_0 + \hat{m}_0^2/2}\right)$, where σ_{cluster}, m_0 and $\hat{m}_0$ are constants defined in [10]. The cluster and array arrival models are identical to those in the GSV structure except that the number of cluster arrivals is a Poisson RV with mean $\bar{L}$, contrary to the nonrestricted case in (2). However, the following analytical results based on (2) can still be applied to some of the IEEE 802.15.4a channel models, as will be clarified in Section V. It is noticed that each of the IEEE UWB channel models is abstracted from rich channel measurements and shall best represent the channel ensemble of certain scenarios, e.g., see [6], [9], [11], and references therein. Therefore, the following analytical results can also reflect the performance tendency of DS-UWB systems in various real-world UWB channels.

The discrete-time baseband channel coefficients $\{h[n]\}_{n=0}^{L-1}$ can then be obtained by

$$\begin{aligned} h[n] &= \int_{-\infty}^{\infty} g(nT - t) h(t) e^{-j\omega_c t} dt \\ &= \sum_{l \geq 0} \sum_{k \geq 0} g(nT - T_l - \tau_{k,l}) \alpha(T_l, \tau_{k,l}) e^{-j\omega_c (T_l + \tau_{k,l})} \end{aligned} \tag{8}$$

where T is the chip duration of the DS-UWB system and $g(t) = \int_{-\infty}^{\infty} p(u) p(u - t) du$ is the composite response of the pulse shaping function $p(t)$ and the matched function $p(-t)$ at the receiver. We may assume that $g(t)$ is real-valued and satisfies $g(0) = 1$, corresponding to unit pulse energy. The term $e^{-j\omega_c t}$ stands for the down-conversion process for passband channel models, e.g., those in [8], with $\omega_c = 2\pi f_c$ and f_c the carrier center frequency. Note that we should have $\omega_c = 0$ for the case with baseband channel models [7], [10]. Finally, the value of Ω_0 will be properly chosen so that

$$\sum_{n=0}^{L-1} E\{|h[n]|^2\} = 1$$

and that of L denotes the largest tap index with tap energy above a threshold of the ignorable value. Regarding the multiple-access, we assume that different users experience independent channel realizations from a common channel model.

III. SINR Expression at the Rake Receiver Ouput

In this section, the effect of ISI, MAI, and noise will be investigated. The SINR expression before being averaged over the channel statistics will be obtained. We start by expanding (1) into the following terms:

$$\begin{aligned} Z = d_0 \cdot & \sum_{i=0}^{N_f - 1} |h[i]|^2 + \sum_{i=0}^{L-1} \sum_{l=0, l \neq i}^{L-1} \tilde{h}^*[i] h[l] \\ & \cdot \sum_{n=0}^{N_c - 1} d_{\lfloor (n-l+i)/N_c \rfloor} c^*[n] c[n - l + i] \\ & + \sum_{\nu=2}^{N_u} \sum_{i=0}^{L-1} \sum_{l=0}^{L-1} \tilde{h}^*[i] h^{(\nu)}[l] \\ & \cdot \sum_{n=0}^{N_c - 1} d^{(\nu)}_{\lfloor (n-l+i)/N_c \rfloor} c^*[n] c^{(\nu)}[n - l + i] \end{aligned}$$

[3] This assumption is actually not too restrictive as it will be seen that these two ratios are indeed constant for the UWB channel models of interest, namely, the considered IEEE 802.15.3a and IEEE 802.15.4a models.

[4] Although the IEEE 802.15.4a channel structure allows a different value of m for the first ray in each cluster, which makes that r_4 in (5) may not be a constant, we notice that it is not implemented in the concerned IEEE 802.15.4a channel models [10].

$$+\sum_{i=0}^{L-1}\tilde{h}^*[i]\sum_{n=0}^{N_c-1}c^*[n]\eta[n+i]$$
$$=d_0\cdot\sum_{i=0}^{N_f-1}|h[i]|^2+Z_{\rm ISI}+\sum_{\nu=2}^{N_u}Z_{\rm MAI}^{(\nu)}+Z_\eta$$

where the first term denotes the desired signal and the remainders correspond to ISI, MAI, and noise. We can define the average output SINR as in [14] by

$$\frac{E_s\cdot\left(E\left\{\sum_{i=0}^{N_f-1}|h[i]|^2\right\}\right)^2}{E\left\{\left|Z-d_0\cdot\sum_{i=0}^{N_f-1}|h[i]|^2\right|^2\right\}}$$
$$=\frac{E_s\cdot\left(\sum_{i=0}^{N_f-1}E\left\{|h[i]|^2\right\}\right)^2}{E\left\{|Z_{\rm ISI}|^2\right\}+\sum_{\nu=2}^{N_u}E\left\{\left|Z_{\rm MAI}^{(\nu)}\right|^2\right\}+E\left\{|Z_\eta|^2\right\}}\quad(9)$$

where the expectation is over the random data and channel statistics and the equality follows from the fact that the interference and noise terms are uncorrelated of zero mean. As a companion metric, the amount of fading [15], [32] defined by

$$\mathrm{AF}=\frac{\mathrm{Var}\left\{\sum_{i=0}^{N_f-1}|h[i]|^2\right\}}{\left(E\left\{\sum_{i=0}^{N_f-1}|h[i]|^2\right\}\right)^2}\quad(10)$$

will also be considered, and a smaller value of AF indicates less relative variation in the combined channel energy and thus better signal quality. For the case without ISI and MAI, (10) can coincide with the original definition in [32], i.e., $\mathrm{Var}\{\mathrm{SNR}_o\}/(E\{\mathrm{SNR}_o\})^2$, where SNR_o is the output signal-to-noise ratio at the Rake combiner output.

The ISI effect for DS-SS systems with low spreading gain has been investigated in [27] and [28] where random spreading sequences are commonly assumed. In this paper, we can, however, obtain an expression for the ISI power as a function of the employed spreading sequence, which can then be used to evaluate and optimize the spreading sequence design by looking at the resulting interference power. Define the two periodic code correlation functions as in [27]

$$R_c^{(1,\nu)}[m]=\sum_{n=0}^{(-m-1)\bmod N_c}c^*[n]c^{(\nu)}[n+m]$$
$$\hat{R}_c^{(1,\nu)}[m]=\sum_{n=(-m-1)\bmod N_c+1}^{N_c-1}c^*[n]c^{(\nu)}[n+m]$$

and the channel-related correlation functions of higher-order cross moments as shown in the equation at the bottom of the page, where the expectation is over the channel statistics. Then, we can obtain (11), as shown at the bottom of the next page, where $\Re\{\cdot\}$ denotes the real part of its entry. Similar to the derivation for (11), the normalized MAI power can also be obtained as in (12), shown at the bottom of the next page. Finally, direct calculation results in

$$\frac{E\left\{|Z_\eta|^2\right\}}{E_s}=\frac{N_0}{E_s}\cdot\sum_{n=0}^{N_c-1}\sum_{n'=0}^{N_c-1}c^*[n]c[n']\cdot\sum_{l=0}^{N_f-1}E\left\{h[l]h^*[l+n'-n]\right\}\quad(13)$$

and then the average output SINR can be obtained from (9)–(13). From (11)–(13), it can be observed that the output interference and noise powers are functions of the correlation functions of both the spreading sequences and channel taps. In contrast to the UWB systems with sparse pulses, as considered

---

$$R_{h,1}^{(1,\nu)}[m,m']=\begin{cases}\sum_{n=m}^{L-1}\sum_{n'=m'}^{L-1}E\left\{\tilde{h}^*[n]h^{(\nu)}[n-m]\tilde{h}[n']h^{(\nu)*}[n'-m']\right\}, & \lfloor\frac{m}{N_c}\rfloor=\lfloor\frac{m'}{N_c}\rfloor\\ 0, & \text{otherwise}\end{cases}$$
$$\hat{R}_{h,1}^{(1,\nu)}[m,m']=\begin{cases}\sum_{n=m}^{L-1}\sum_{n'=m'}^{L-1}E\left\{\tilde{h}^*[n]h^{(\nu)}[n-m]\cdot\tilde{h}[n']h^{(\nu)*}[n'-m']\right\}, & \lfloor\frac{m}{N_c}\rfloor=\lfloor\frac{m'}{N_c}\rfloor+1\\ 0, & \text{otherwise}\end{cases}$$
$$R_{h,2}^{(1,\nu)}[m,m']=\begin{cases}\sum_{n=m}^{L-1}\sum_{n'=m'}^{L-1}E\left\{\tilde{h}^*[n-m]h^{(\nu)}[n]\tilde{h}[n'-m']h^{(\nu)*}[n']\right\}, & \lceil\frac{m}{N_c}\rceil=\lceil\frac{m'}{N_c}\rceil\\ 0, & \text{otherwise}\end{cases}$$
$$\hat{R}_{h,2}^{(1,\nu)}[m,m']=\begin{cases}\sum_{n=m}^{L-1}\sum_{n'=m'}^{L-1}E\left\{\tilde{h}^*[n-m]h^{(\nu)}[n]\tilde{h}[n'-m']h^{(\nu)*}[n']\right\}, & \lceil\frac{m}{N_c}\rceil=\lceil\frac{m'}{N_c}\rceil-1\\ 0, & \text{otherwise}\end{cases}$$
$$\tilde{R}_h^{(1,\nu)}[m,m']=\sum_{n=m}^{L-1}\sum_{n'=m'}^{L-1}E\left\{\tilde{h}^*[n]h^{(\nu)}[n-m]\tilde{h}[n'-m']h^{(\nu)*}[n']\right\}$$

in [22]–[24], the pulses/chips of DS-UWB systems are close in succession and thus the suppression of the output interference relies heavily on the design of the spreading sequence. Although low autocorrelation side-lobes and low cross-correlations of the spreading sequences generally give smaller values of (11) and (12), the effect of the channel correlations should be considered as well. Consequently, the obtained equations, regarding the joint effects of the spreading sequence and channel, can be particularly useful in obtaining the best sequence(s) from a set of candidates, as will be demonstrated in Section V.

IV. Exact Average SINR Over GSV Channel Structure

Careful examination indicates that computation of (9)–(13) requires evaluation of $E\left\{|h[n]|^2\right\}$, $E\{h[n_1]h^*[n_2]\}$, and the generic form $E\left\{h[n_1]h^*[n_2]h^{(\nu)}[n_3]h^{(\nu)*}[n_4]\right\}$ (for all the channel-related correlation functions and other related quantities). We first note that

$$E\left\{|h[n]|^2\right\} = E\{h[n_1]h^*[n_2]\}\big|_{n_1=n_2=n} \tag{14}$$

and, by the assumption that all users' channels are independent but generated from a common model, we can have

$$E\left\{h[n_1]h^*[n_2]h^{(\nu)}[n_3]h^{(\nu)*}[n_4]\right\} = E\{h[n_1]h^*[n_2]\}\cdot E\{h[n_3]h^*[n_4]\}$$

if $\nu \neq 1$. Consequently, it suffices to consider the two-tap correlation, $E\{h[n_1]h^*[n_2]\}$, and the four-tap correlation, $E\{h[n_1]h^*[n_2]h[n_3]h^*[n_4]\}$. It is noticed that, for IEEE 802.15.3a channels, the two-tap correlation with generic $g(t)$ can be obtained from [20], while, in the following subsections, we are able to provide extended results for the GSV channels. The four-tap correlation for IEEE 802.15.3a channels can be found from [15] when an idealized rectangular $g(t)$ is assumed. We can, however, derive exact results for the GSV channels with generic pulse shaping functions. The key to the desired results is the analytical framework based on the useful properties of renewal processes, as will be introduced in the following subsection.

$$\begin{aligned}\frac{E\left\{|Z_{\mathrm{ISI}}|^2\right\}}{E_s} &= \sum_{m=1}^{L-1}\sum_{m'=1}^{L-1} R_{h,1}^{(1,1)}[m,m']\left(R_c^{(1,1)}[m]R_c^{(1,1)*}[m'] + \hat{R}_c^{(1,1)}[m]\hat{R}_c^{(1,1)*}[m']\right)\\ &\quad + \sum_{m=1}^{L-1}\sum_{m'=1}^{L-1} R_{h,2}^{(1,1)}[m,m']\left(R_c^{(1,1)}[-m]R_c^{(1,1)*}[-m'] + \hat{R}_c^{(1,1)}[-m]\hat{R}_c^{(1,1)*}[-m']\right)\\ &\quad + 2\Re\Bigg\{\sum_{m=1}^{L-1}\sum_{m'=1}^{L-1}\hat{R}_{h,1}^{(1,1)}[m,m']R_c^{(1,1)}[m]\hat{R}_c^{(1,1)*}[m']\\ &\qquad + \sum_{m=1}^{N_c-1}\sum_{m'=1}^{N_c-1}\cdot\tilde{R}_h^{(1,1)}[m,m']R_c^{(1,1)}[m]\hat{R}_c^{(1,1)*}[-m']\\ &\qquad + \sum_{m=1}^{L-1}\sum_{m'=1}^{L-1}\hat{R}_{h,2}^{(1,1)}[m,m']R_c^{(1,1)}[-m]\hat{R}_c^{(1,1)*}[-m']\Bigg\}\end{aligned} \tag{11}$$

$$\begin{aligned}\frac{E\left\{\left|Z_{\mathrm{MAI}}^{(\nu)}\right|^2\right\}}{E_s} &= \sum_{m=0}^{L-1}\sum_{m'=0}^{L-1} R_{h,1}^{(1,\nu)}[m,m']\left(R_c^{(1,\nu)}[m]R_c^{(1,\nu)*}[m'] + \hat{R}_c^{(1,\nu)}[m]\hat{R}_c^{(1,\nu)*}[m']\right)\\ &\quad + \sum_{m=1}^{L-1}\sum_{m'=1}^{L-1} R_{h,2}^{(1,\nu)}[m,m']\left(R_c^{(1,\nu)}[-m]R_c^{(1,\nu)*}[-m'] + \hat{R}_c^{(1,\nu)}[-m]\hat{R}_c^{(1,\nu)*}[-m']\right)\\ &\quad + 2\Re\Bigg\{\sum_{m=0}^{L-1}\sum_{m'=0}^{L-1}\hat{R}_{h,1}^{(1,\nu)}[m,m']R_c^{(1,\nu)}[m]\hat{R}_c^{(1,\nu)*}[m']\\ &\qquad + \sum_{m=0}^{N_c-1}\sum_{m'=1}^{N_c-1}\tilde{R}_h^{(1,\nu)}[m,m']R_c^{(1,\nu)}[m]\hat{R}_c^{(1,\nu)*}[-m']\\ &\qquad + \sum_{m=1}^{L-1}\sum_{m'=1}^{L-1}\hat{R}_{h,2}^{(1,\nu)}[m,m']R_c^{(1,\nu)}[-m]\hat{R}_c^{(1,\nu)*}[-m']\Bigg\}.\end{aligned} \tag{12}$$

A. Properties of Renewal Processes

In a Poisson process, the time durations between successive occurrences of a concerned event are i.i.d. exponential RVs. When the inter-arrival time follows a common generic distribution, we can obtain a renewal process, where an event occurrence is called a renewal [25], [26]. It is clear that the cluster arrival and ray arrival processes in a GSV channel can both be described by renewal processes. We first recall some useful results from [25] and [26].

Definition 1 (Renewal Function and Renewal Density [26]): Consider a renewal process, $\{N(t), t \geq 0\}$, with inter-arrival time pdf $f(x)$. The renewal function, denoted by $M(x)$, is defined as the mean number of renewals in $(0, x]$, i.e.,

$$M(x) = E\{N(x)\}.$$

The first derivative of $M(x)$ with respect to x is called the renewal density, denoted by $m(x)$.

One useful property of $m(x)$ is that $m(x)dx$ corresponds to the probability that *one* renewal occurs in $(x, x+dx)$[25], [26]. Since the probability of more than two renewals in $(x, x+dx)$ vanishes as dx approaches zero if $f(x)$ does not degenerate to $\delta(x)$, it turns out that $m(x)$ corresponds to the *instantaneous rate* of a renewal process at time x. It should be noted that $m(x)$ is not a pdf in x since

$$\lim_{t\to\infty}\int_{x=0}^{t} m(x)dx = \lim_{t\to\infty} E\{N(t)\} = \infty.$$

Yet the probability nature in $m(x)$ still allows manipulations as for pdfs. In addition, $m(x)$ can be obtained from $f(x)$ by the following relation [26]:

Lemma 1: Let $m(x)$ be the renewal density of a renewal process with inter-arrival time pdf $f(x)$; then $m(x)$ can be obtained from $f(x)$ by

$$\mathcal{L}\{m(x)\} = \frac{\mathcal{L}\{f(x)\}}{1-\mathcal{L}\{f(x)\}}$$

where $\mathcal{L}\{\cdot\}$ stands for the Laplace transform.

Note that $m(x)$ defined above does not include the possible arrival at $x = 0$, which can, however, be present in the cluster and ray arrival processes of a GSV channel. To accommodate this phenomenon, we will consider the extended renewal density (ERD) $\tilde{m}(x)$ such that $\tilde{m}(x)dx$ corresponds to the probability that there is a renewal in $[x, x+dx)$. Now, with Lemma 1, we can further obtain the following two useful lemmas:

Lemma 2: Let $\tilde{m}_c(x)$ be the ERD of the cluster arrival process in a GSV channel with inter-arrival time pdf given by (6). Then

$$\tilde{m}_c(x) = \Lambda + \delta(x) I_{\text{LOS}} \tag{15}$$

where $I_E = 1$ if the event E in the subscript is present and zero, otherwise.

Proof: When there is no LOS, the cluster arrival process is exactly an ordinary Poisson process with rate Λ. Then, by Lemma 1 and (6), it can be shown that

$$\tilde{m}_c(x) = \Lambda.$$

When LOS is present, there is always a cluster arrival at time 0, which then contributes to the second term in (15). ■

Lemma 3: Let $\tilde{m}_{r|c}(y|x)$ be the conditional ERD of the ray-arrival process, given that its cluster begins at x, in a GSV channel with inter-arrival time pdf given by (7). Then

$$\tilde{m}_{r|c}(y|x) = \lambda + ce^{-(y-x)/\mu} + \delta(y-x) \tag{16}$$

where $\mu = 1/[(1-\beta)\lambda_1 + \beta\lambda_2]$, $c = \beta(1-\beta)(\lambda_1-\lambda_2)^2\mu$, and $\lambda = \lambda_1\lambda_2\mu$.

Proof: Ignoring the ray arrival whenever a cluster begins, we can have that the ray-arrival process is an ordinary renewal process with inter-arrival time pdf $f_r(x)$ given in (7). Then, by the fact that the ray arrival process only depends on the time difference to its start time, we first have

$$\tilde{m}_{r|c}(y|x) = m_r(y-x)$$

where $m_r(x)$ is the renewal density obtained from $f_r(x)$. By Lemma 1, one can obtain that

$$m_r(y-x) = \lambda + ce^{-(y-x)/\mu}$$

with μ, c, and λ defined above. The last term in (16) occurs since there is *always* a ray whenever a cluster begins. ■

Notably, (16) reveals that the ERD of the ray arrival process can decrease with time when $\beta \neq 1$, which provides additional flexibility for channel modeling as utilized in [10]. On the other hand, if $\beta = 1$, one can simply set $c = 0$ in the following analytical results.

B. Two-Tap Correlation

Now, with the above properties, the two-tap correlation can be obtained as obtained by

$$\begin{aligned}
&E\{h[n_1]h^*[n_2]\} \\
&\overset{(a)}{=} E\Bigg\{\sum_{l\geq 0}\sum_{k\geq 0}\sum_{l'\geq 0}\sum_{k'\geq 0} g(n_1T - T_l - \tau_{k,l}) \\
&\qquad \cdot g(n_2T - T_{l'} - \tau_{k',l'})\alpha(T_l,\tau_{k,l})\alpha^*(T_{l'},\tau_{k',l'}) \\
&\qquad \cdot e^{-j\omega_c(T_l+\tau_{k,l}-T_{l'}-\tau_{k',l'})}\Bigg\} \\
&\overset{(b)}{=} E\Bigg\{\sum_{l\geq 0}\sum_{k\geq 0} g(n_1T - T_l - \tau_{k,l}) \\
&\qquad \cdot g(n_2T - T_l - \tau_{k,l})\left|\alpha(T_l,\tau_{k,l})\right|^2\Bigg\} \\
&\overset{(c)}{=} \int_0^\infty\int_0^t E\Bigg\{g(n_1T-t)g(n_2T-t) \\
&\qquad \cdot |\alpha(s,t-s)|^2 \,\Bigg|\, \begin{array}{l}\text{a cluster in } [s, s+ds) \\ \text{with a ray in } [t, t+dt)\end{array}\Bigg\} \\
&\qquad \cdot \tilde{m}_{r|c}(t|s)\,\tilde{m}_c(s)dsdt \\
&\overset{(d)}{=} \int_0^\infty g(n_1T-t)g(n_2T-t)\cdot\int_0^t \Omega_0 e^{-s/\Gamma}e^{-(t-s)/\gamma} \\
&\qquad \cdot\left[\lambda + ce^{-(t-s)/\mu} + \delta(t-s)\right][\Lambda + \delta(s)I_{\text{LOS}}]\,dsdt
\end{aligned}$$

where the equality (a) follows from (8), (b) is by the path-gain assumption in (3), (c) represents the calculation conditioned over all possible cluster and ray arrival times, and (d) is obtained by (3), Lemma 2, and Lemma 3. After evaluating the above equation, we can arrive at the following proposition:

Proposition 1: Consider a discrete-time baseband channel converted from a GSV channel according to (8), and then the cross-correlation of two channel taps $h[n_1]$ and $h[n_2]$ is given by

$$\begin{aligned} &E\{h[n_1]h^*[n_2]\} \\ &\quad = \Omega_0\Lambda\left[\lambda\rho B_{n_1,n_2}(\gamma,0) + (1-\lambda\rho)B_{n_1,n_2}(\Gamma,0)\right] \\ &\qquad + \Omega_0\Lambda c\check{\rho}\left[B_{n_1,n_2}(\check{\gamma},0) - B_{n_1,n_2}(\Gamma,0)\right] \\ &\qquad + I_{\mathrm{LOS}}\cdot\Omega_0\left[\lambda B_{n_1,n_2}(\gamma,0) + cB_{n_1,n_2}(\check{\gamma},0)\right. \\ &\qquad\qquad \left. + g(n_1T)g(n_2T)\right] \end{aligned} \tag{17}$$

where $\rho = (1/\Gamma - 1/\gamma)^{-1}$, $\check{\gamma} = (1/\gamma + 1/\mu)^{-1}$, $\check{\rho} = (1/\Gamma - 1/\check{\gamma})^{-1}$, and

$$B_{m,n}(\xi,\omega_c) = \int_0^\infty g(mT-t)g(nT-t)e^{-t/\xi}e^{-j2\omega_c t}dt. \tag{18}$$

C. Four-Tap Correlation

For the four-tap correlation, we first observe the first equation shown at the bottom of the page. Then, by removing the terms with zero contributions due to the assumption on the

$$\begin{aligned} &E\{h[n_1]h^*[n_2]h[n_3]h^*[n_4]\} \\ &\quad = E\Bigg\{\sum_{l_1\geq 0}\sum_{k_1\geq 0}\sum_{l_2\geq 0}\sum_{k_2\geq 0}\sum_{l_3\geq 0}\sum_{k_3\geq 0}\sum_{l_4\geq 0}\sum_{k_4\geq 0}\alpha(T_{l_1},\tau_{k_1,l_1})\alpha^*(T_{l_2},\tau_{k_2,l_2})\alpha(T_{l_3},\tau_{k_3,l_3})\alpha^*(T_{l_4},\tau_{k_4,l_4}) \\ &\qquad \cdot g(n_1T - T_{l_1} - \tau_{k_1,l_1})g(n_2T - T_{l_2} - \tau_{k_2,l_2})g(n_3T - T_{l_3} - \tau_{k_3,l_3})g(n_4T - T_{l_4} - \tau_{k_4,l_4}) \\ &\qquad \cdot e^{-j\omega_c\left(T_{l_1}+\tau_{k_1,l_1}-T_{l_2}-\tau_{k_2,l_2}+T_{l_3}+\tau_{k_3,l_3}-T_{l_4}-\tau_{k_4,l_3}\right)}\Bigg\}. \end{aligned}$$

$$\begin{aligned} E\{h[n_1]h^*[n_2]h[n_3]h^*[n_4]\} &= E\Bigg\{\sum_{l_1\geq 0}\sum_{k_1\geq 0}\sum_{l_3\geq 0}\sum_{k_3\geq 0} g(n_1T - T_{l_1} - \tau_{k_1,l_1}) \\ &\qquad \cdot g(n_2T - T_{l_1} - \tau_{k_1,l_1})g(n_3T - T_{l_3} - \tau_{k_3,l_3}) \\ &\qquad \cdot g(n_4T - T_{l_3} - \tau_{k_3,l_3})\left|\alpha(T_{l_1},\tau_{k_1,l_1})\right|^2\left|\alpha(T_{l_3},\tau_{k_3,l_3})\right|^2\Bigg\} \\ &\quad + E\Bigg\{\sum_{l_1\geq 0}\sum_{k_1\geq 0}\sum_{l_2\geq 0}\sum_{k_2\geq 0} g(n_1T - T_{l_1} - \tau_{k_1,l_1}) \\ &\qquad \cdot g(n_3T - T_{l_1} - \tau_{k_1,l_1})g(n_2T - T_{l_2} - \tau_{k_2,l_2}) \\ &\qquad \cdot g(n_4T - T_{l_2} - \tau_{k_2,l_2})\left(\alpha(T_{l_1},\tau_{k_1,l_1})\right)^2\left(\alpha^*(T_{l_2},\tau_{k_2,l_2})\right)^2 \\ &\qquad \cdot e^{-j2\omega_c\left(T_{l_1}+\tau_{k_1,l_1}-T_{l_2}-\tau_{k_2,l_2}\right)}\Bigg\} \\ &\quad + E\Bigg\{\sum_{l_1\geq 0}\sum_{k_1\geq 0}\sum_{l_2\geq 0}\sum_{k_2\geq 0} g(n_1T - T_{l_1} - \tau_{k_1,l_1}) \\ &\qquad \cdot g(n_4T - T_{l_1} - \tau_{k_1,l_1})g(n_2T - T_{l_2} - \tau_{k_2,l_2}) \\ &\qquad \cdot g(n_3T - T_{l_2} - \tau_{k_2,l_2})\left|\alpha(T_{l_1},\tau_{k_1,l_1})\right|^2\left|\alpha(T_{l_2},\tau_{k_2,l_2})\right|^2\Bigg\} \\ &\quad + E\Bigg\{\sum_{l\geq 0}\sum_{k\geq 0} g(n_1T - T_l - \tau_{k,l})g(n_2T - T_l - \tau_{k,l}) \\ &\qquad \cdot g(n_3T - T_l - \tau_{k,l})g(n_4T - T_l - \tau_{k,l})\left|\alpha(T_l,\tau_{k,l})\right|^4\Bigg\} \end{aligned} \tag{19}$$

fourth-order joint moment of path gains, one can obtain (19), as shown at the bottom of the previous page, where either the cluster arrival times or the ray arrival times are distinct in the first three terms. For the path gains defined in [7] and [10], $E\left\{(\alpha(T_l,\tau_{k,l}))^2\right\} = 0$, for all k, l, and the second term vanishes. But, for the real-valued path gains in [8], $E\left\{(\alpha(T_l,\tau_{k,l}))^2\right\} = E\left\{\left|\alpha(T_l,\tau_{k,l})\right|^2\right\}$ and we may denote and rewrite the second term as

$$\begin{aligned}
&P_2(n_1,n_3,n_2,n_4,\omega_c)\\
&\quad= E\Bigg\{\sum_{l_1\geq 0}\sum_{k_1\geq 0}\sum_{l_2\geq 0}\sum_{k_2\geq 0} g(n_1T-T_{l_1}-\tau_{k_1,l_1})\\
&\qquad\cdot g(n_3T-T_{l_1}-\tau_{k_1,l_1})g(n_2T-T_{l_2}-\tau_{k_2,l_2})\\
&\qquad\cdot g(n_4T-T_{l_2}-\tau_{k_2,l_2})\left|\alpha(T_{l_1},\tau_{k_1,l_1})\right|^2\\
&\qquad\cdot\left|\alpha(T_{l_2},\tau_{k_2,l_2})\right|^2 e^{-j2\omega_c\left(T_{l_1}+\tau_{k_1,l_1}-T_{l_2}-\tau_{k_2,l_2}\right)}\Bigg\}.
\end{aligned}\tag{20}$$

Now, since the first and third terms in (19) are equal to $P_2(n_1,n_2,n_3,n_4,0)$ and $P_2(n_1,n_4,n_2,n_3,0)$, respectively, it suffices to evaluate (20), which is accomplished in the Appendix.

Denote the last term in (19) by $P_4(n_1,n_2,n_3,n_4)$, and then it can be evaluated in a similar way as for the two-tap correlation, as shown in the equation at the bottom of the page, where r_4 is defined in (5). For clarity, further define

$$\begin{aligned}
&B_{n_1,n_2,n_3,n_4}(\xi)\\
&= \int_0^\infty g(n_1T-t)g(n_2T-t)g(n_3T-t)g(n_4T-t)e^{-t/\xi}dt
\end{aligned}$$

and then, after some calculations, we can obtain

$$\begin{aligned}
&P_4(n_1,n_2,n_3,n_4)\\
&\quad= r_4\Omega_0^2\Lambda\Bigg[\lambda\rho_1 B_{n_1,n_2,n_3,n_4}\left(\frac{\gamma}{2}\right)\\
&\qquad+(1-\lambda\rho_1)B_{n_1,n_2,n_3,n_4}\left(\frac{\Gamma}{2}\right)\Bigg]\\
&\qquad+ r_4\Omega_0^2\Lambda c\rho_2\Bigg[B_{n_1,n_2,n_3,n_4}\left(\left(\frac{2}{\gamma}+\frac{1}{\mu}\right)^{-1}\right)\\
&\qquad- B_{n_1,n_2,n_3,n_4}\left(\frac{\Gamma}{2}\right)\Bigg] + I_{\mathrm{LOS}}\\
&\qquad\cdot r_4\Omega_0^2\Bigg[\lambda B_{n_1,n_2,n_3,n_4}\left(\frac{\gamma}{2}\right)\\
&\qquad+ cB_{n_1,n_2,n_3,n_4}\left(\left(\frac{2}{\gamma}+\frac{1}{\mu}\right)^{-1}\right)\\
&\qquad+ g(n_1T)g(n_2T)g(n_3T)g(n_4T)\Bigg]
\end{aligned}\tag{21}$$

where $\rho_1 = (2/\Gamma - 2/\gamma)^{-1}$ and $\rho_2 = (2/\Gamma - 2/\gamma - 1/\mu)^{-1}$. In summary, we have the following proposition:

Proposition 2: Consider a discrete-time baseband channel converted from a GSV channel by (8), and then the cross-correlation of four channel taps $h[n_1]$, $h[n_2]$, $h[n_3]$, and $h[n_4]$ is given by

$$\begin{aligned}
&E\left\{h[n_1]h^*[n_2]h[n_3]h^*[n_4]\right\}\\
&\quad= P_2(n_1,n_2,n_3,n_4,0) + P_2(n_1,n_3,n_2,n_4,\omega_c)\\
&\qquad+ P_2(n_1,n_4,n_2,n_3,0) + P_4(n_1,n_2,n_3,n_4)
\end{aligned}$$

where $P_2(m,n,m',n',\omega_c)$ and $P_4(n_1,n_2,n_3,n_4)$ can be obtained from (24) and (21), respectively.

V. Numerical and Simulation Results

A. Application to IEEE Channel Models

The application of the above analytical results to IEEE 802.15.3a channel models in [8] is straightforward by setting $c = 0$ and substituting corresponding values to other parameters, while it is not the case for IEEE 802.15.4a channel models [10] as mentioned in Section II-B. The number of cluster arrivals of a GSV channel, if we restrict $0 \leq T_l < T_{\mathrm{trunc}}$, becomes a Poisson RV with mean $\Lambda T_{\mathrm{trunc}} + I_{\mathrm{LOS}}$. On the other

---

$$\begin{aligned}
P_4(n_1,n_2,n_3,n_4) &= \int_0^\infty\int_0^t E\Bigg\{g(n_1T-t)g(n_2T-t)g(n_3T-t)g(n_4T-t)\\
&\qquad\cdot\left|\alpha(s,t-s)\right|^4\Bigg|\begin{array}{l}\text{a cluster in } [s,s+ds)\\ \text{with a ray in } [t,t+dt)\end{array}\Bigg\}\\
&\quad\cdot\tilde{m}_{r|c}(t|s)\tilde{m}_c(s)dsdt\\
&= \int_0^\infty g(n_1T-t)g(n_2T-t)g(n_3T-t)g(n_4T-t)\\
&\quad\cdot\int_0^t r_4\left(\Omega_0 e^{-s/\Gamma}e^{-(t-s)/\gamma}\right)^2\\
&\quad\cdot\left[\lambda + ce^{-(t-s)/\mu}+\delta(t-s)\right]\cdot\left[\Lambda+\delta(s)I_{\mathrm{LOS}}\right]ds\,dt
\end{aligned}$$

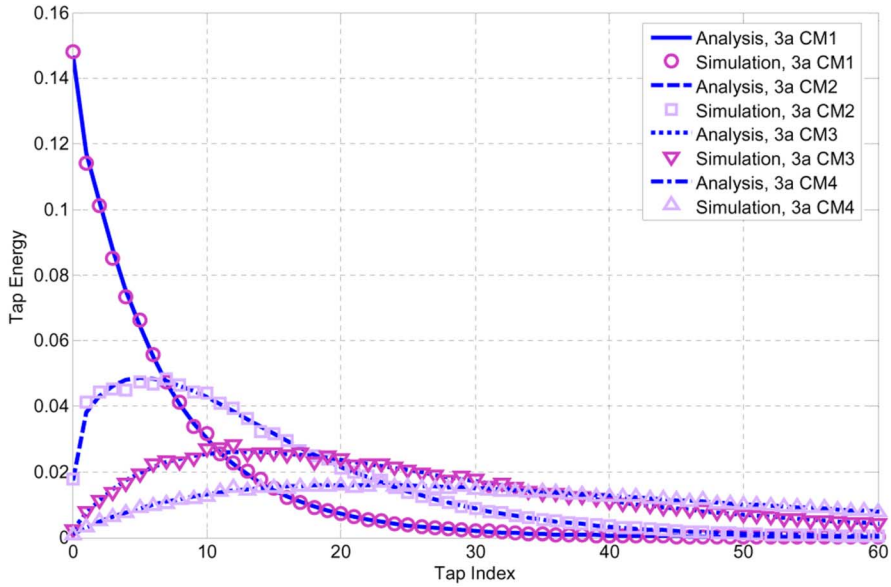

Fig. 1. Average tap energy for IEEE 802.15.3a channel models with chip duration $T = 0.769$ ns and root-raised-cosine pulse function of roll-off factor 0.3.

TABLE I
VALUES OF $M = (\bar{L} - I_{\mathrm{LOS}})/(\Lambda\Gamma)$ FOR THE IEEE 802.15.4A CHANNEL MODELS

Model	L	Λ	Γ	$M = (L - I_{\mathrm{LOS}})/(\Lambda\Gamma)$
CM1	3	0.047	22.61	1.882
CM2	3.5	0.12	26.27	1.110
CM3	5.4	0.016	14.60	18.836
CM5	13.6	0.0448	31.70	8.872
CM6	10.5	0.0243	104.70	4.127
CM9	3.31	0.0305	56.00	1.938

hand, channel realizations generated from the channel models of clustering phenomena in [10] take the following format:

$$h(t) = \sum_{l=0}^{L_c-1} \sum_{k\geq 0} \alpha(T_l, \tau_{k,l})\delta(t - T_l - \tau_{k,l})$$

where L_c is a Poisson RV with mean $\bar{L}$ but there is no restriction on T_l. For a GSV channel to give the same average number of clusters, we shall restrict $0 \leq T_l < T_{\mathrm{trunc}} = (\bar{L} - I_{\mathrm{LOS}})/\Lambda$. Since the cluster power decreases exponentially with time, a cluster arriving at T_l becomes ignorable if $T_l \geq M\Gamma$ with Γ the cluster decay factor and M not too small, which effectively corresponds to $T_{\mathrm{trunc}} = M\Gamma$. Consequently, for IEEE 802.15.4a channel models with $M = (\bar{L} - I_{\mathrm{LOS}})/(\Lambda\Gamma)$ not too small, our analytical results should be able to provide good predictions, as will be verified in the following subsection. Since this value of M is obtained by matching the the mean cluster number of the cluster arrival process over $[0, M\Gamma)$ to $\bar{L}$, it follows that, for an IEEE 802.15.4a channel model with M very small, cluster arrivals may essentially appear within the confined time interval $[0, M\Gamma)$ and the average energy is expected to be relatively more concentrated on the front taps than that of the corresponding GSV model. Table I summarizes the values of M for IEEE 802.15.4a channel models, excluding CM4, CM7, and CM8 of different structures from the GSV model.

B. Performance Evaluation and Comparison

In this subsection, performance results of DS-UWB systems over IEEE UWB channels will be presented, along with simulation results to verify our analysis. For IEEE 802.15.3a channels, we assume a DS-UWB system with carrier center frequency of 3.9 GHz, chip duration $T = 0.769$ ns, and a root-raised-cosine pulse shaping function of roll-off factor 0.3, as used in [13]. Since the DS-SS scheme is not adopted by the IEEE 802.15.4a Task Group [33], we will test another system configuration, which can also demonstrate that our analytical results are valid for wide ranges of system parameters. Therefore, for IEEE 802.15.4a channels, we will consider chip duration $T = 2$ ns, roll-off factor 0.5, and particularly discuss the value of M, which may affect the accuracy of our analysis.

The analytical results of the average tap energy given by (14) and (17) with IEEE 802.15.3a CM1, CM2, CM3, and CM4 channel parameters specified in [8] are first compared with computer simulations. For each channel model, 10000 channel realizations are averaged in the simulations, and the comparisons are given in Fig. 1. As observed, the analytical results well match the simulations. For IEEE 802.15.4a channel models: CM1, CM2, CM3, CM5, CM6, and CM9, the analytical and simulation results for average tap energy are compared in Fig. 2. As shown, when $M > 4$, our analytical results can give close predictions; while the average energy of 4a channels with M really small is more concentrated on the front taps, as expected. The simulated SINR performance of the DS-UWB systems with a single user and three co-channel users are also provided to verify our analytical results regarding interferences. Assume the following additional configurations: $E_b/N_0 = 15$ dB, binary phase-shift keying (BPSK) data modulation, the first spreading sequence of $N_c = 12, 6$ specified in [13] for the single-user case and the first three sequences of $N_c = 24, 12$ for the multi-user case, Rake receiving with finger number $N_f = 3n$, for $n = 1, 2, 3, \ldots$, and 10 000 channel realizations tested for each user. Then, comparisons

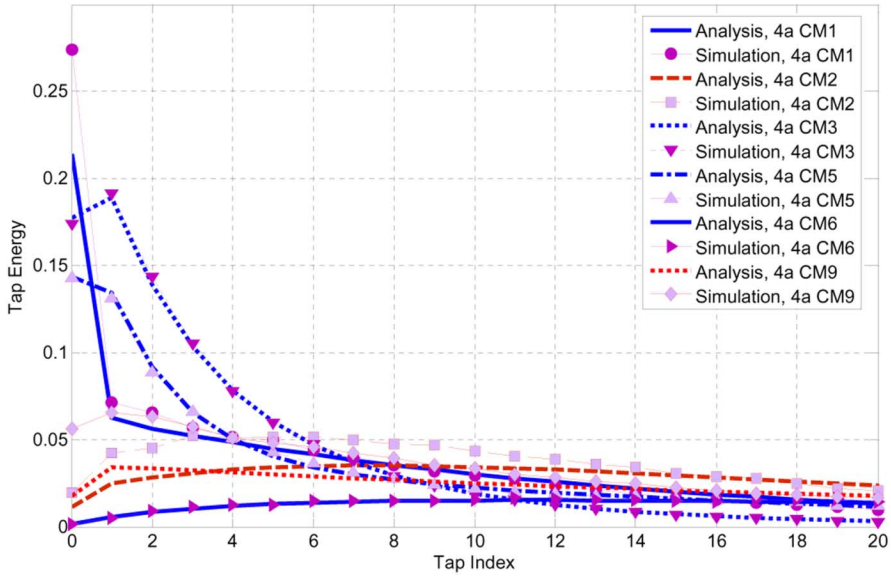

Fig. 2. Average tap energy for IEEE 802.15.4a CM1, CM2, CM3, CM5, CM6, and CM9 channel models with chip duration $T = 2$ ns and root-raised-cosine pulse function of roll-off factor 0.5.

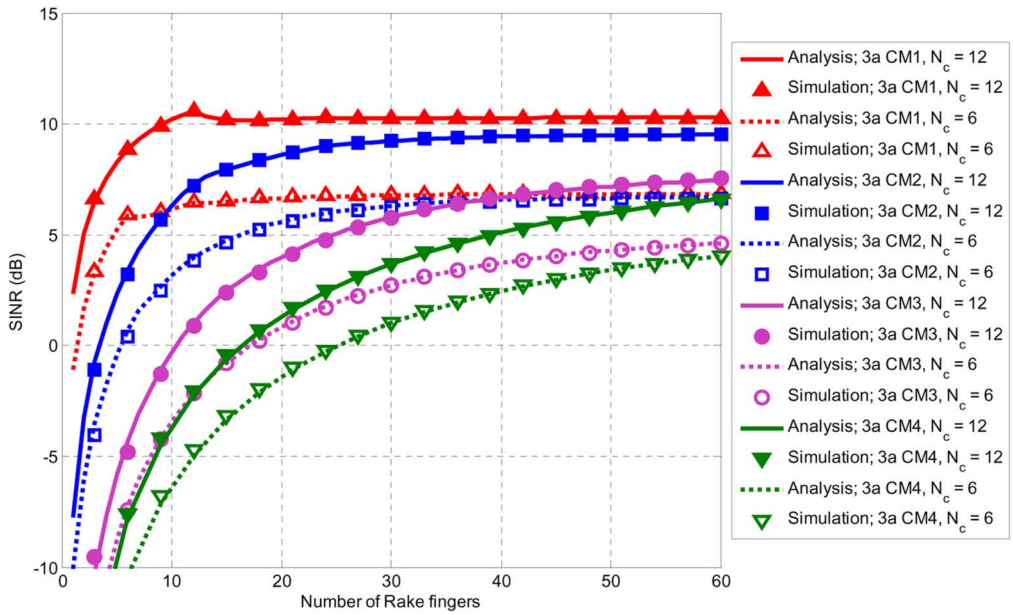

Fig. 3. Average output SINR versus the number of Rake fingers for a DS-UWB system with a single user over IEEE 802.15.3a channels.

of analytical and simulation results over IEEE 802.15.3a CM1 (with LOS) and CM2 to CM4 (without LOS) are given in Figs. 3 and 4 for the single-user and multi-user cases, respectively. It is clear that our analytical results agree with computer simulations very well. For the curves of CM1 in the single-user case, it is interesting to note that choosing $N_f = 12$ suffices to approach the optimal SINR. In fact, with the sequence of $N_c = 12$, more fingers can even degrade the performance due to the resulting severe ISI by the short period of the spreading sequence. This phenomena has, however, not been revealed in previous related works ignoring ISI [14]–[17]. The analytical and simulated curves for AF are also collected in Fig. 5, where 30000 channel realizations are averaged for each simulated curve. Together with Figs. 3 and 4, it can be observed that the number of Rake fingers to reach most of the asymptotic SINR values can be considerably small for channels with LOS, while one can obtain better AF values over CM2 and CM4 channels than those for CM1 with more Rake fingers. An immediate application is now evident that one can readily determine the number of Rake fingers with the best trade-off among SINR, AF, and receiver complexity by evaluating the average output SINR and AF versus the number of Rake fingers according to our analytical results.

For IEEE 802.15.4a channels, we may consider CM3, CM5 (with LOS), and CM6 (without LOS) with $M > 4$, under which our analytical results are expected to give good estimates. For SINR simulations, the same additional configurations as for IEEE 802.15.3a channels are assumed, and comparisons with

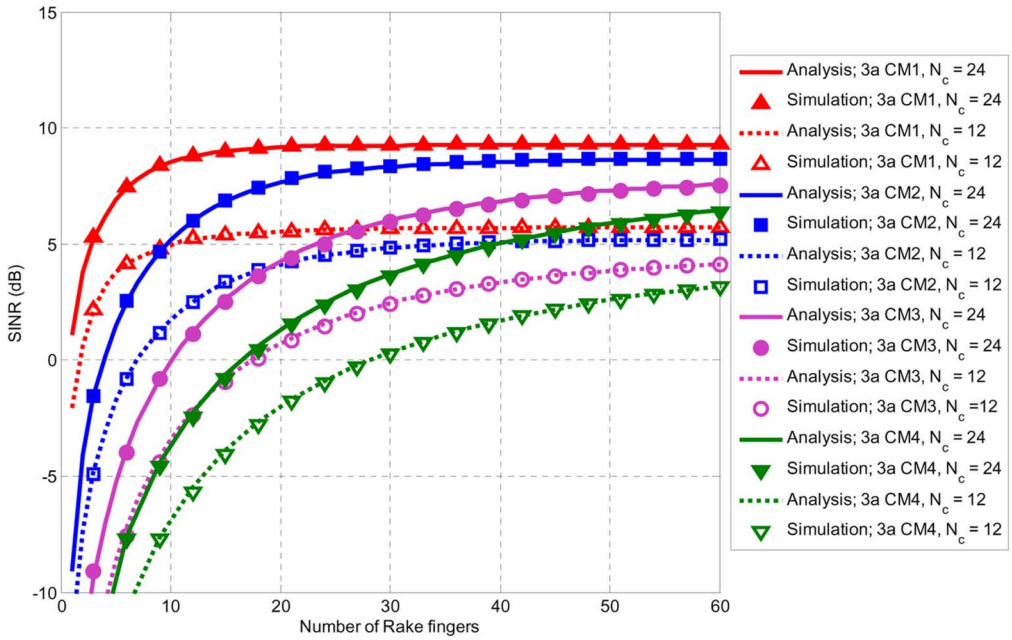

Fig. 4. Average output SINR versus the number of Rake fingers for a DS-UWB system with three users over IEEE 802.15.3a channels.

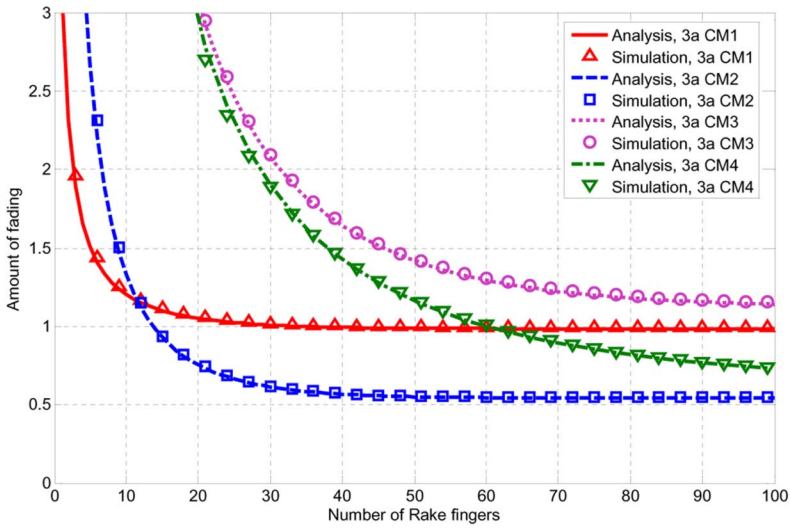

Fig. 5. Amount of fading versus the number of Rake fingers over IEEE 802.15.3a channels.

the analytical results for the single-user and multi-user cases are shown in Figs. 6 and 7, respectively. As observed, our analytical results can reach good agreement with the simulations. For AF curves given in Fig. 8, the agreement is weaker for CM5 and CM6 with smaller values of M. But the deviations are not large and the tendencies have essentially been catched.

C. Finding the Best Spreading Sequence

An alternative application of our analytical results is to find the best spreading sequence regarding the joint effect of the sequence and channel, as noted at the end of Section III. For the demonstration purpose, we consider the length-6 and length-12 sequences for the single-user scenario over IEEE 802.15.3a CM1 and CM2 channels. Assume a ternary alphabet, $\{-A, 0, A\}$, for each sequence entry where A is a scalar for normalization of the sequence energy; then there are totally $3^6 - 1$ and $3^{12} - 1$ nonzero length-6 and length-12 candidates, respectively. According to the previous SINR and AF results, we can pick out the sequences that give the best and the second-best SINR values with 12 and 24 Rake fingers for CM1 and CM2 channels. Table II summaries the found sequences with the achieved SINRs. Note that only the representative sequences are given in the table and other equivalent sequences giving the same SINR values can be obtained by circularly shifting the representatives or multiplying them by -1. It is interesting to note that the best sequences are of the same type, i.e., there is only one nonzero entry. In addition, the best length-6 sequence and the second-best length-12 sequences for the CM1 channel turn out to be identical to those adopted in [13].

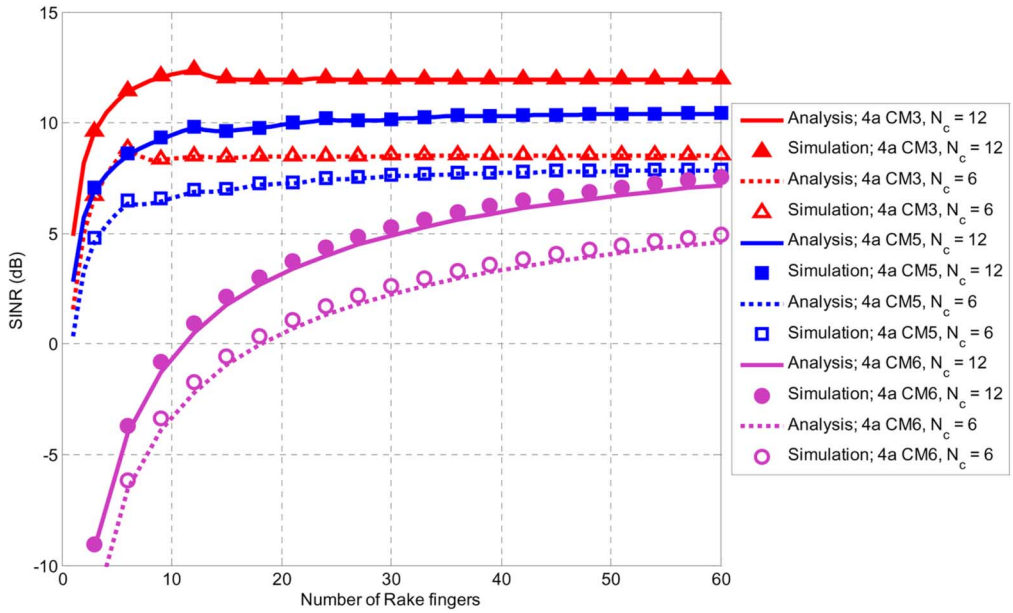

Fig. 6. Average output SINR versus the number of Rake fingers for a DS-UWB system with a single user over IEEE 802.15.4a CM3, CM5, and CM6 channels.

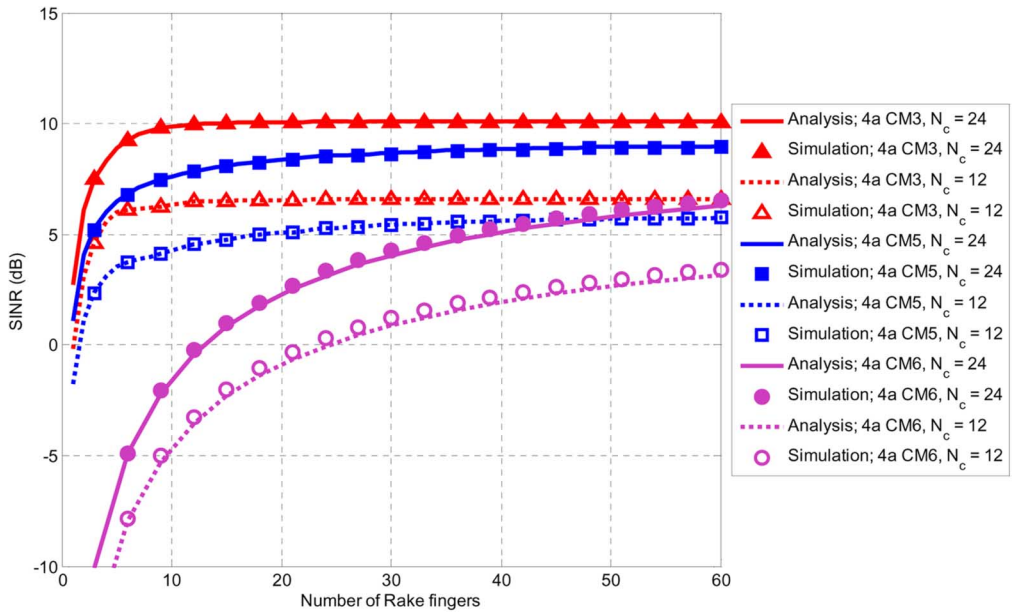

Fig. 7. Average output SINR versus the number of Rake fingers for a DS-UWB system with three users over IEEE 802.15.4a CM3, CM5, and CM6 channels.

VI. Concluding Remarks

In this paper, we have derived an exact analytical expression of the average output SINR for a DS-UWB system with Rake receiving in the presence of ISI and MAI over the GSV channels. The novel treatment of the renewal processes is the key for the analytical results. Computer simulations have verified the accuracy of our analysis over different channel and system configurations. The obtained analytical results can readily be applied to performance prediction/evaluation and system optimization over realistic channel and interference models, such as determination of the number of Rake fingers with the best tradeoff among SINR, AF, and receiver complexity, finding the best spreading sequences, etc.

It should be noticed that, although synchronized multiple access is assumed in the paper, the analytical results can, in fact, be extended to the asynchronous case by first imposing the multiple-access random delays in (2) and adjusting the discrete-time baseband channels in (8) for the co-channel users. Then, the extension will only involve the modification of the co-channel users' two-tap correlation functions required in the formula of the MAI power. For the concern of the applicability of our analytical results in real-world UWB channels that may not be well described by the IEEE UWB channel models, performance evaluation can still be carried out by computing (9)–(13) with the channel correlation functions obtained through averaging the channel measurement data whenever they are available.

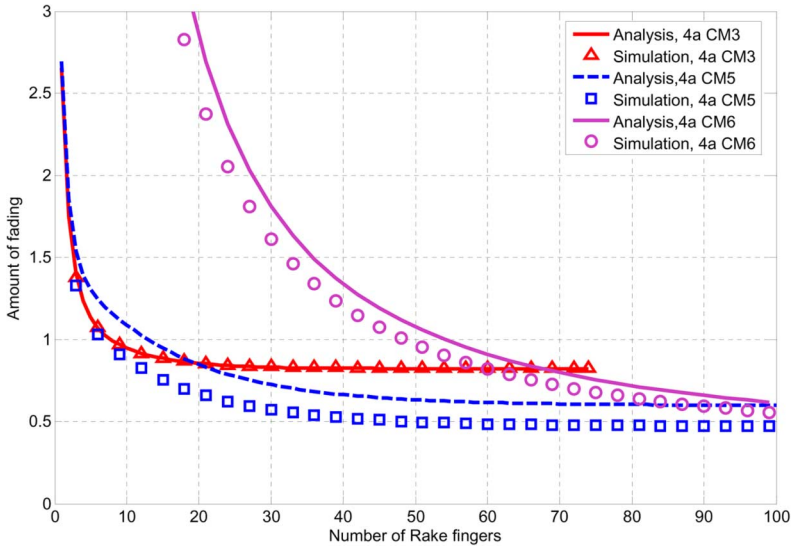

Fig. 8. Amount of fading versus the number of Rake fingers over IEEE 802.15.4a CM3, CM5, and CM6 channels.

TABLE II
SELECTED REPRESENTATIVE SEQUENCES

Sequence Length	Channel Model	SINR	Representative Sequence(s)
6	CM1	6.44	$(-1\ 0\ 0\ 0\ 0\ 0)$
		5.86	$(-1\ 1\ -1\ -1\ -1\ 0) \times \sqrt{1/5}$
			$(-1\ -1\ -1\ 1\ -1\ 0) \times \sqrt{1/5}$
6	CM2	5.97	$(-1\ 0\ 0\ 0\ 0\ 0)$
		5.68	$(-1\ 1\ -1\ -1\ -1\ 0) \times \sqrt{1/5}$
			$(-1\ -1\ -1\ 1\ -1\ 0) \times \sqrt{1/5}$
12	CM1	11.37	$(-1\ 0\ 0\ 0\ 0\ 0\ 0\ 0\ 0\ 0\ 0\ 0)$
		10.59	$(-1\ -1\ -1\ 1\ 1\ 1\ -1\ 1\ 1\ -1\ 1\ 0) \times \sqrt{1/11}$
			$(-1\ 1\ -1\ -1\ 1\ -1\ -1\ -1\ 1\ 1\ 1\ 0) \times \sqrt{1/11}$
12	CM2	9.50	$(-1\ 0\ 0\ 0\ 0\ 0\ 0\ 0\ 0\ 0\ 0\ 0)$
		9.04	$(-1\ 1\ -1\ -1\ -1\ 0\ 0\ 0\ 0\ 0\ 0\ 0) \times \sqrt{1/5}$
			$(-1\ -1\ -1\ 1\ -1\ 0\ 0\ 0\ 0\ 0\ 0\ 0) \times \sqrt{1/5}$

APPENDIX
EVALUATION OF $P_2(n_1, n_3, n_2, n_4, \omega_c)$

We first separate the evaluation of (20) into two cases, namely, $T_l \neq T_{l'}$ and $T_l = T_{l'}$ but $\tau_{k,l} \neq \tau_{k',l'}$, which corresponds to cases that the two distinct rays in (20) belong to different clusters or a common cluster. Denote the corresponding contributions by $P_2^{(d)}(n_1, n_3, n_2, n_4, \omega_c)$ and $P_2^{(c)}(n_1, n_3, n_2, n_4, \omega_c)$, respectively. Then, for the former contribution, let the ray at t_i belong to the cluster at s_i with $0 \leq s_i \leq t_i$, $i = 1, 2$, and $s_1 \neq s_2$, and let $\tilde{m}(t_1, s_1, t_2, s_2)$ denote the joint ERD. Restricting to $s_1 < s_2$ and noting the probability nature of the ERD, we can have

$$\begin{aligned}
&\tilde{m}(t_1, s_1, t_2, s_2) I_{[s_1 < s_2]} \\
&\quad = [\tilde{m}(t_2|t_1, s_1, s_2) \cdot \tilde{m}(t_1|s_1, s_2) \cdot \tilde{m}(s_2|s_1) \cdot \tilde{m}_c(s_1)] \\
&\qquad \cdot I_{[s_1 < s_2]} \\
&\quad = \left[\tilde{m}_{r|c}(t_2|s_2) \cdot \tilde{m}_{r|c}(t_1|s_1) \cdot \tilde{m}_c(s_2) I_{[s_2 > 0]} \cdot \tilde{m}_c(s_1)\right] \\
&\qquad \cdot I_{[s_1 < s_2]}
\end{aligned}$$

where $\tilde{m}(\cdot|\cdot)$ is an abbreviated notation for the conditional ERD and the last equality follows from the fact that t_1 and t_2 only depend on s_1 and s_2, respectively, and, by the Markovian property of the cluster arrival process, $\tilde{m}(s_2|s_1) = \tilde{m}_c(s_2 - s_1) = \Lambda = \tilde{m}_c(s_2) I_{[s_2 > 0]}$. By symmetry,

$$\begin{aligned}
&\tilde{m}(t_1, s_1, t_2, s_2) I_{[s_1 > s_2]} \\
&\quad = \left[\tilde{m}_{r|c}(t_1|s_1) \cdot \tilde{m}_{r|c}(t_2|s_2) \cdot \tilde{m}_c(s_1) I_{[s_1 > 0]} \cdot \tilde{m}_c(s_2)\right] \\
&\qquad \cdot I_{[s_1 > s_2]}.
\end{aligned}$$

Now, conditioned over all possible cluster and ray arrival times, $P_2^{(d)}(n_1, n_3, n_2, n_4, \omega_c)$ can be found to be

$$\begin{aligned}
&\int_0^\infty \int_{\substack{0 \\ t_1 \neq t_2}}^\infty g(n_1 T - t_1) g(n_3 T - t_1) \\
&\quad \cdot g(n_2 T - t_2) g(n_4 T - t_2) e^{-j 2\omega_c (t_1 - t_2)} \\
&\quad \cdot \int_0^{t_2} \int_0^{t_1} \Omega_0 e^{-s_1/\Gamma} e^{-(t_1 - s_1)/\gamma} \cdot \Omega_0 e^{-s_2/\Gamma} e^{-(t_2 - s_2)/\gamma} \\
&\quad \cdot \left(\tilde{m}(t_1, s_1, t_2, s_2) I_{[s_1 < s_2]} + \tilde{m}(t_1, s_1, t_2, s_2) I_{[s_1 > s_2]}\right) \\
&\quad \cdot ds_1 ds_2 dt_1 dt_2 \\
&\qquad = \Omega_0^2 C_{n_1, n_3}(\omega_c) C_{n_2, n_4}(-\omega_c) + I_{\text{LOS}} \\
&\qquad\quad \cdot \Omega_0^2 \Big[C_{n_1, n_3}(\omega_c) \Big(\lambda B_{n_2, n_4}(\gamma, -\omega_c) \\
&\qquad\qquad + c B_{n_2, n_4}(\breve{\gamma}, -\omega_c) + g(n_2 T) g(n_4 T) \Big)
\end{aligned}$$

$$\int_0^\infty \int_{\substack{0\\ t_1\neq t_2}}^\infty g(n_1T-t_1)g(n_3T-t_1)g(n_2T-t_2)g(n_4T-t_2)e^{-j2\omega_c(t_1-t_2)}$$
$$\cdot \int_0^\infty r_2\cdot\Omega_0 e^{-s/\Gamma}e^{-(t_1-s)/\gamma}\cdot\Omega_0 e^{-s/\Gamma}e^{-(t_2-s)/\gamma}$$
$$\cdot\left(\tilde{m}(t_1,t_2,s)I_{[t_1<t_2]}+\tilde{m}(t_1,t_2,s)I_{[t_1>t_2]}\right)dsdt_1dt_2$$
$$= r_2\Omega_0^2\Lambda\Bigg(\lambda(1-\lambda\rho_1-c\rho_2)D_{n1,n3,n2,n4}(\gamma,\omega_c)+c(1-\lambda\rho_2-c\check{\rho_1})D_{n1,n3,n2,n4}(\check{\gamma},\omega_c)$$
$$+\lambda c\rho_2\left[B_{n_1,n_3}(\gamma,w_c)+B_{n_1,n_3}(\check{\gamma},w_c)\right]\left[B_{n_2,n_4}(\gamma,-w_c)+B_{n_2,n_4}(\check{\gamma},-w_c)\right]$$
$$+\lambda(\lambda\rho_1-c\rho_2)B_{n_1,n_3}(\gamma,w_c)B_{n_2,n_4}(\gamma,-w_c)+c(c\check{\rho_1}-\lambda\rho_2)B_{n_1,n_3}(\check{\gamma},w_c)B_{n_2,n_4}(\check{\gamma},-w_c)\Bigg)$$
$$+I_{\mathrm{LOS}}\cdot r_2\Omega_0^2\Bigg(\left[\lambda B_{n_1,n_3}(\gamma,w_c)+cB_{n_1,n_3}(\check{\gamma},w_c)\right]\left[\lambda B_{n_2,n_4}(\gamma,-w_c)+cB_{n_2,n_4}(\check{\gamma},-w_c)\right]$$
$$+g(n_1T)g(n_3T)\Big[\lambda B_{n_2,n_4}(\gamma,-w_c)+cB_{n_2,n_4}(\check{\gamma},-w_c)\Big]$$
$$+\Big[\lambda B_{n_1,n_3}(\gamma,w_c)+cB_{n_1,n_3}(\check{\gamma},w_c)\Big]g(n_2T)g(n_4T)\Bigg) \tag{23}$$

$$+\left(\lambda B_{n_1,n_3}(\gamma,\omega_c)+cB_{n_1,n_3}(\check{\gamma},\omega_c)\right.$$
$$\left.+g(n_1T)g(n_3T)\right)C_{n_2,n_4}(-\omega_c)\Big] \tag{22}$$

where the restriction $t_1\neq t_2$ is ignored since the integrand is integrable in $\mathbb{R}^2$ and the support of $\{t_1\neq t_2\}$ is of zero measure. In addition, $B_{m,n}(\cdot,\cdot)$ is defined in (18) and

$$C_{m,n}(\omega_c)=\Lambda\left[\lambda\rho B_{m,n}(\gamma,\omega_c)+(1-\lambda\rho)B_{m,n}(\Gamma,\omega_c)\right]$$
$$+\Lambda c\check{\rho}\left[B_{m,n}(\check{\gamma},\omega_c)-B_{m,n}(\Gamma,\omega_c)\right].$$

For the contribution from a common cluster, let the cluster arrive at time s and $\tilde{m}(t_1,t_2,s)$ be the joint ERD of the cluster and ray arrival times. Restricting to $t_1<t_2$, we have $s\leq t_1<t_2$ and

$$\tilde{m}(t_1,t_2,s)I_{[t_1<t_2]}$$
$$=\left[\tilde{m}_{r|c}(t_2|s)I_{[t_2>s]}\cdot\tilde{m}_{r|c}(t_1|s)\right]I_{[t_1<t_2]}\cdot\tilde{m}_c(s)I_{[s\leq t_1]}$$
$$=\left[\lambda+ce^{-(t_2-s)/\mu}\right]\left[\lambda+ce^{-(t_1-s)/\mu}+\delta(t_1-s)\right]$$
$$\cdot I_{[t_1<t_2]}\cdot\left[\Lambda+\delta(s)I_{\mathrm{LOS}}\right]I_{[s\leq t_1]}.$$

By symmetry

$$\tilde{m}(t_1,t_2,s)I_{[t_1>t_2]}$$
$$=\left[\lambda+ce^{-(t_1-s)/\mu}\right]\left[\lambda+ce^{-(t_2-s)/\mu}+\delta(t_2-s)\right]$$
$$\cdot I_{[t_1>t_2]}\cdot\left[\Lambda+\delta(s)I_{\mathrm{LOS}}\right]I_{[s\leq t_2]}.$$

Again, similarly, $P_2^{(c)}(n_1,n_3,n_2,n_4,\omega_c)$ can be found to be as shown in (23), at the top of the page, where the restriction $t_1\neq t_2$ is also ignored by the same reason as for $P_2^{(d)}(n_1,n_3,n_2,n_4,\omega_c)$ and r_2 is defined in (4) and introduced since rays at t_1 and t_2 have the same cluster effect. Besides, $\rho_1=(2/\Gamma-2/\gamma)^{-1}$, $\check{\rho_1}=(2/\Gamma-2/\check{\gamma})^{-1}$, $\rho_2=(2/\Gamma-2/\gamma-1/\mu)^{-1}$, and

$$D_{n_1,n_3,n_2,n_4}(\xi,\omega_c)$$
$$=\int_0^\infty\int_0^\infty g(n_1T-t_1)g(n_3T-t_1)$$
$$\cdot g(n_2T-t_2)g(n_4T-t_2)$$
$$\cdot e^{-j2\omega_c(t_1-t_2)}e^{-|t_1-t_2|/\xi}e^{-2\min(t_1,t_2)/\Gamma}dt_1dt_2.$$

In summary

$$P_2(n_1,n_3,n_2,n_4,\omega_c)$$
$$=P_2^{(d)}(n_1,n_3,n_2,n_4,\omega_c)+P_2^{(c)}(n_1,n_3,n_2,n_4,\omega_c) \tag{24}$$

where $P_2^{(d)}(n_1,n_3,n_2,n_4,\omega_c)$ and $P_2^{(c)}(n_1,n_3,n_2,n_4,\omega_c)$ are given by (22) and (23), respectively.

ACKNOWLEDGMENT

The authors are grateful to the anonymous reviewers for their comments and suggestions that were incorporated into the paper.

REFERENCES

[1] Federal Communication Commission, Revision of Part 15 of the Commission's Rules Regarding Ultra-Wideband Transmission Systems 2002, ET-Docket 98-153.

[2] M. Z. Win and R. A. Scholtz, "Characterization of ultra-wide bandwidth wireless indoor channels: A communication-theoretic view," *IEEE J. Select. Areas Commun.*, vol. 20, no. 12, pp. 1613–1627, Dec. 2002.

[3] M. Ghavami, L. B. Michael, and R. Kohno, *Ultra Wideband Signals and Systems in Communication Engineering*. New York: Wiley, 2004.

[4] L. Yang and G. B. Giannakis, "Ultra-wideband communications: An idea whose time has come," *IEEE Signal Process. Mag.*, vol. 21, no. 6, pp. 26–54, Nov. 2004.

[5] R. C. Qiu, H. Liu, and X. Shen, "Ultra-wideband for multiple access communications," *IEEE Commun. Mag.*, vol. 43, no. 2, pp. 80–87, Feb. 2005.
[6] A. F. Molisch, "Ultrawideband propagation channels-theory, measurement, and modeling," *IEEE Trans. Veh. Technol.*, vol. 54, no. 5, pp. 1528–1545, Sep. 2005.
[7] A. Saleh and R. Valenzuela, "A statistical model for indoor multipath propagation," *IEEE J. Select. Areas Commun.*, vol. SAC-5, no. 2, pp. 128–137, Feb. 1987.
[8] J. Foerster *et al.*, Channel Modeling Sub-Committe Rep. Final 2003, IEEE doc.: IEEEP802.15-02/490r1-SG3a.
[9] A. F. Molisch, J. R. Foerster, and M. Pendergrass, "Channel models for ultrawideband personal area networks," *IEEE Wireless Commun.*, vol. 10, no. 6, pp. 14–21, Dec. 2003.
[10] A. F. Molisch *et al.*, IEEE 802.15.4a Channel Model-Final Rep. 2005, IEEE doc.: IEEE 802.15-04-0662-02-004a.
[11] A. F. Molisch, D. Cassioli, C.-C. Chong, S. Emami, A. Fort, B. Kannan, J. Karedal, J. Kunisch, H. G. Schantz, K. Siwiak, and M. Z. Win, "A comprehensive standardized model for ultrawideband propagation channels," *IEEE Trans. Antennas Propagat.*, vol. 54, no. 11, pp. 3151–3166, Nov. 2006.
[12] M. Z. Win and R. A. Scholtz, "Ultra-wide bandwidth time-hopping spread-spectrum impulse radio for wireless multiple access communications," *IEEE Trans. Commun.*, vol. 48, no. 4, pp. 679–689, Apr. 2000.
[13] R. Fisher, R. Kohno, M. M. Laughlin, and M. Welborn, DS-UWB Physical Layer Submission to 802.15 Task Group 3a 2004, IEEE doc.: IEEEP802.15-04/0137r3.
[14] T. Jia and D. I. Kim, "Analysis of average signal-to-interference-noise ratio for indoor UWB rake receiving system," in *Proc. IEEE Vehicular Technology Conf.*, Stockholm, Sweden, May 2005, pp. 1396–1400.
[15] K. Hao and J. A. Gubner, "Performance measures and statistical quantities of rake receivers using maximal-ratio combining on the IEEE 802.15.3a UWB channel model," *IEEE Trans. Wireless Commun.*, submitted for publication.
[16] J. A. Gubner and K. Hao, "A computable formula for the average bit error probability as a function of window size for the IEEE 802.15.3a UWB channel model," *IEEE Trans. Microwave Theory Tech.*, vol. 54, no. 6, pp. 1762–1768, Jun. 2006.
[17] W.-C. Liu and L.-C. Wang, "Performance analysis of pulse based ultra-wideband systems in the highly frequency selective fading channel with cluster property," in *Proc. IEEE Vehicular Technology Conf.*, Melbourne, Australia, May 2006, pp. 1459–1463.
[18] W.-C. Liu and L.-C. Wang, "BER analysis of the IEEE 802.15.4a channel model with rake receiver," in *Proc. IEEE Vehicular Technology Conf.*, Montreal, Canada, Sep. 2006, pp. 1–5.
[19] K. Hao and J. A. Gubner, "The distribution of sums of path gains in the IEEE 802.15.3a UWB channel model," *IEEE Trans. Wireless Commun.*, vol. 6, no. 3, pp. 811–816, Mar. 2007.
[20] J. A. Gubner and K. Hao, "The IEEE 802.15.3a UWB channel model as a two-dimensional augmented cluster process," *IEEE Trans. Inform. Theory*, submitted for publication.
[21] T. Q. S. Quek and M. Z. Win, "Analysis of UWB transmitted-reference communication systems in dense multipath channels," *IEEE J. Select. Areas Commun.*, vol. 23, no. 9, pp. 1863–1874, Sep. 2005.
[22] K. Witrisal, M. Pausini, and A. Trindade, "Multiuser interference amnd interfram interference in UWB transmitted reference systems," in *Proc. Int. Workshop Ultra Wideband Systems Joint Conf. Ultrawideband System Tech.*, Kyoto, Japan, May 2004, pp. 96–100.
[23] K. Witrisal and M. Pausini, "Impact of multipath propagation on impulse radio UWB autocorrelation receivers," in *Proc. IEEE Int. Conf. Ultra-Wideband*, Zurich, Switzerland, Sep. 2005, pp. 485–490.
[24] K. Witrisal and M. Pausini, "Statistical analysis of UWB channel correlation functions," *IEEE Trans. Veh. Technol.*, to be published.
[25] S. M. Ross, *Stochastic Processes*. New York: Wiley, 1996.
[26] E. P. C. Kao, *An Introduction to Stochastic Processes*. Belmont, CA: Duxbury, 1997.
[27] C. Unger and G. P. Fettweis, "Analysis of the rake receiver performance in low spreading gain DS/SS systems," in *Proc. IEEE Global Telecommunications Conf.*, Taipei, Taiwan, Nov. 2002, pp. 830–834.
[28] K. Huang, F. Adachi, and Y. H. Chew, "A more accurate analysis of interference for rake combining on DS-CDMA forward link in mobile radio," *IEICE Trans. Commun.*, vol. E88-B, pp. 654–663, Feb. 2005.
[29] C.-C. Lee, W.-D. Wu, and C.-C. Chao, "Signal-to-interference-plus-noise ratio analysis for direct-sequence ultra-wideband systems," in *Proc. IEEE Wireless Commun. Network Conf.*, Hong Kong, Mar. 2007, pp. 1763–1767.
[30] Y.-W. Hong and A. Scaglione, "Time synchronization and reach-back communications with pulse-coupled oscillators for UWB wireless ad hoc networks," in *Proc. IEEE Int. Conf. Ultra-Wideband Systems Tech.*, Reston, VA, Nov. 2003, pp. 190–194.
[31] X. Luo and G. B. Giannakis, "Raise your voice at a proper pace to synchronize in multiple ad hoc piconets," *IEEE Trans. Signal Process.*, vol. 55, no. 6, pp. 267–278, Jun. 2007.
[32] M. K. Simon and M. Alouini, *Digital Communication Over Fading Channels: A Unified Approach to Performance Analysis*, 2nd ed. New York: Wiley, 2005.
[33] G. M. Maggio, TG4a UWB-PHY Overview 2005, IEEE doc.: IEEEP802.15-05/0707r1.

Wei-De Wu (S'03) was born in Taipei, Taiwan, R.O.C., in 1979. He received the B.S. degree in electrical engineering in 2001 from the National Tsing Hua University, Hsinchu, Taiwan, R.O.C., where he is currently pursuing the Ph.D. degree with the Institute of Communications Engineering.

His research interests include ultra-wideband communications, signal processing for wireless communications, and information theory.

Cheng-Chia Lee was born in Taipei, Taiwan, R.O.C., in 1981. He received the B.S. degree in electrical engineering and the M.S. degree in communications engineering from the National Tsing Hua University, Hsinchu, Taiwan, R.O.C., in 2004 and 2006, respectively.

Since January 2007, he has been with Sunplus Mobile, Inc., Hsinchu, Taiwan, where he currently works in the Communication Development Division. His research interests include digital communications and signal processing.

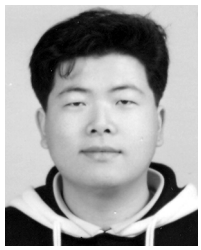

Chung-Hsuan Wang (S'94–M'01) received the B.S. and Ph.D. degrees from the National Tsing Hua University, Hsinchu, Taiwan, R.O.C., in 1994 and 2001, respectively, both in electrical engineering.

From August 2001 to July 2004, he held a faculty position in the Department of Electronic Engineering, Chung Yuan Christian University, Chung-Li, Taiwan. Since August 2004, he has been an Assistant Professor with the Department of Communication Engineering, National Chiao Tung University, Hsinchu. His research interests include wireless communications, error-correcting codes, information theory, and signal processing.

Chi-chao Chao (S'87–M'89) was born in Taipei, Taiwan, R.O.C., in 1961. He received the B.S. degree from the National Taiwan University, Taipei, Taiwan, R.O.C., in 1983 and the M.S. and Ph.D. degrees from the California Institute of Technology (Caltech), Pasadena, in 1986 and 1989, respectively, all in electrical engineering.

He was an instructor in the Department of Weapon Command and Control Systems, Naval Weapon School, Kaohsiung, Taiwan, during his military service from 1983 to 1985. Since September 1989, he has been with the National Tsing Hua University (NTHU), Hsinchu, Taiwan, where he is currently a Professor in the Department of Electrical Engineering and the Institute of Communications Engineering. He has also served as the Director of the Institute of Communications Engineering, NTHU, since August 2005. He held visiting positions at Caltech from September 1995 to March 1996 and at Bell Communications Research (now Telcordia Technologies), Morristown, NJ, from March 1996 to August 1996. His current research interests include digital communications, error-correcting codes, information theory, and wireless networks.

Dr. Chao was the Secretary of the IEEE Taipei Section from 1997 to 1998 and the Chairman of the IEEE Information Theory Society Taipei Chapter from 1999 to 2001. He served as an Associate Editor for the IEEE Communications Letters from 2002 to 2005. He received the Distinguished Teaching Award from NTHU in 1993 and 2002.